May 2018

The Allocation of Micro-grid Energy Storage System Considering Controlling Parameter

Ting Hu
University of Wisconsin-Milwaukee

THE ALLOCATION OF MICROGRID ENERGY STORAGE SYSTEM

CONSIDERING CONTROLLING PARAMETER

by
Ting Hu

A Thesis Submitted in
Partial Fulfillment of the
Requirements for the Degree of

Master of Science
in Engineering

at
The University of Wisconsin-Milwaukee
May 2018

ABSTRACT

THE ALLOCATION OF MICROSOFT ENERGY STORAGE SYSTEM CONSIDERING CONTROLLING PARAMETER

by

Ting Hu

The University of Wisconsin-Milwaukee, 2018
Under the Supervision of Pro. David Yu

This research proposes a novel method of how to integrate controlling parameters, voltage and frequency, into to the energy storage system (ESS) allocation in a microgrid with renewable sources. The goal is to use the sensitivity analysis to find the most effective bus where the ESS should be in-stored to minimize the fluctuations both in terms of voltage and frequency. Indicators, such as SAIDI and SAIFI, are used to measure system reliability after the optimum size and location of ESS are determined.

TABLE OF CONTENTS

ACKNOWLEDGEMENTS

First, I would like to thank my thesis advisor Pro. Yu, for his patience and generous support. Without his continuous guidance on my research, this thesis would not have been possible. He has deeply touched me with his rigorous attitude toward research and his unwavering commitment to performing high-level research. His professional mentorship throughout my study here will have a profound impact on my future profession.

I would also like to thank Dr. Hu for his time from their busy schedule and his advice in my research. Additionally, I want to express my sincere gratitude to my lab mate, Yanting Zeng for her company and support.

Last but not least, I want to thank my parents for their support and love.

1 Introduction

Nowadays, as the most popular renewable energy source (RES), wind energy has achieved rapid development and growth. The total wind power capacity is expected to reach nearly 2000 GW by 2030 in an advanced scenario, and to supply between 16.7% and 18.8% of global electricity demand [1]. Due to the intermittent nature of wind power, the wind power integration into power systems brings inherent variability and uncertainty. With the flexible charging–discharging characteristics, Energy Storage System (ESS) is considered as an effective tool to enhance the stability and flexibility not only of a specific wind farm, but also of the entire grid.

Several research works have addressed the problem of sizing ESS to reduce the uncertainty associated with wind energy. In [2], the authors presented a probabilistic approach for sizing and siting energy storage in distribution systems to improve the reliability of distribution systems. Other research works have focused on sizing ESS for isolated microgrid applications as in [3], [4]. In [5] and [4], time-series models have been applied to forecast the stochastic nature of system components and determine the optimal ESS operation during a certain period, based on which size of the ESS is optimized. Despite the difficulties associated with forecasting highly stochastic components, such as wind speed, the application of time series models provides an optimal solution that is valid only for the time-series pattern that is applied.

However, few research works have considered the controlling parameter, such as voltage and frequency when planning the allocation of ESS. This research considers the change of system frequency and voltage magnitude of each bus, due to a change in active power at some bus, into the allocation of ESS. In that way, we can find out which buses are relative effective through the sensitivity analysis. and after battery is added to some bus, reliability indexes are used to measure the entire microgrid performance.

2 Microgrid Configuration and Components

In order to accurately study the behavior of the renewable energy systems, wind turbines, and energy storage systems and their effects on the voltage and frequency in a microgrid, a standard 25 kV IEEE 34 bus system is adopted in this paper [6], [7]. Fig. 1 shows the configuration of the microgrid under study [8]. The original system is a 60 Hz, 24.9 kV, 12 MVA mega with different fixed loads connected and no DG on the system. The load types include constant active/reactive power loads and constant distributed impedance loads (three-phase and single-phase). In order to match the properties of the system with a microgrid under construction at Fort Sill, the nominal voltage of the system is changed to 12 kV and other components of the system including loads and line impedances have been scaled accordingly. The base parameters of the system are changed to 12 kV, 6 MVA. The transformer on bus 832 is scaled down to 12 kV/4.16 kV and the two voltage regulators at bus 832 and 814 are also scaled to 6.9 kV, phase voltage. The power ratings of the fixed PQ loads are reduced to half of their original values. The same also applies to the single-phase PQ loads. To scale the constant impedance loads, their impedances are reduced to half. Since the voltage is also half of the original value, their power rating is reduced to half. There are two types of the distribution lines in this system namely, lumped line impedance and distributed line impedance. For the lines with lumped impedance, to keep the same voltage drop, the line impedances have been halved. The case for distributed line impedance is different. Three methods have been considered to modify the line impedances, when scaling from 24.9 kV to 12 kV system: (i) halving the R/L matrix, (ii) halving the length

of lines, and (iii) halving the length of line and quadrupling the capacitance matrix. Methods (i) and (ii) yield similar results but the voltage drop is larger than the original case. Method (iii) cuts the line power flow in half and at the same time keeps the nodal voltages in per unit the same. Therefore, we have used method (iii) to scale the distributed line impedances [9].

After scaling the microgrid, two types of power sources are added: two 750 kW wind turbines, a 1.2 MVA diesel generator. The modeling and capacity design for these sources have been presented in [9]. Two wind turbines are added to Bus 848 and Bus 840, and are also modeled using Power Systems Computer Aided Design (PSCAD) software considering the turbine efficiency factor (CP) and the mechanical and electrical efficiencies. The inverters designed for wind turbines are modeled as current source connected to the microgrid. The natural gas generator is connected on Bus 800 before the static switch. Since it is the main source to regulate the voltage and frequency of the microgrid, the exciter and governor controls are modeled with sufficient details. The other important source which supports microgrid voltage is energy storage, which is added to bus 828 and is developed according to experimental test results [10]. It should be noted this 34-bus distribution system has significant power losses due to long distribution lines. For instance, the line between buses 806 and 814 is 49730 feet long with impedance of 12.56+j12.54 Ohms. In addition, the line between buses 852 and 854 is 18415 feet long with impedance of 6.73 + j4.92 Ohms. These losses require additional generation capacity to supply the demand. The detailed modeling and

capacity design for wind turbine, diesel generator, and energy storage system have been discussed in [9] and [11].

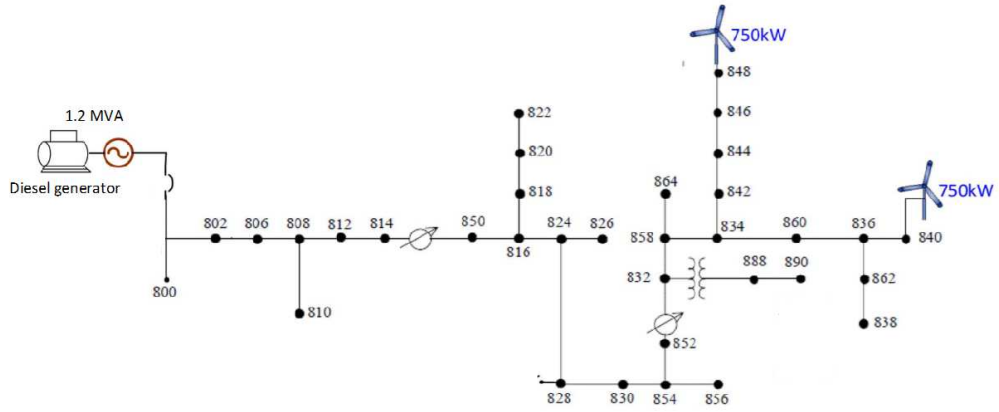

Fig. 2.1 The configuration of the microgrid studied in this research

3 Sensitivity Analysis in electric power system

Newton-Raphson fully coupled method is considered the most general and reliable method to solve the power flow equations which are non-linear. Once the equations for the power flow have been defined, the solution algorithm involves iteration based on successive linearization using the first term of a Taylor expansion of the equations to be solved. Then Jacobean Matrix will be obtained.

Assuming Bus 1 is the swing bus, for n buses system, the Taylor Expansion and Jacobean Matrix will have the following form:

$$\begin{bmatrix} \Delta P_2 \\ \Delta P_3 \\ \text{M} \\ \text{M} \\ \Delta P_n \\ \Delta Q_2 \\ \Delta Q_3 \\ \text{M} \\ \text{M} \\ \Delta Q_n \end{bmatrix} = \begin{bmatrix} \frac{\partial P_2}{\partial \delta_2} & \frac{\partial P_2}{\partial \delta_3} & \text{L} & \frac{\partial P_2}{\partial \delta_n} & \frac{\partial P_2}{\partial |V_2|} & \frac{\partial P_2}{\partial |V_3|} & \text{L} & \frac{\partial P_2}{\partial |V_n|} \\ \frac{\partial P_3}{\partial \delta_2} & \frac{\partial P_3}{\partial \delta_3} & \text{L} & \frac{\partial P_3}{\partial \delta_n} & \frac{\partial P_3}{\partial |V_2|} & \frac{\partial P_3}{\partial |V_3|} & \text{L} & \frac{\partial P_3}{\partial |V_n|} \\ \text{M} & \text{M} & \text{M} & \text{M} & \text{M} & \text{M} & \text{M} & \text{M} \\ \frac{\partial P_n}{\partial \delta_2} & \frac{\partial P_n}{\partial \delta_3} & \text{L} & \frac{\partial P_n}{\partial \delta_n} & \frac{\partial P_n}{\partial |V_2|} & \frac{\partial P_n}{\partial |V_3|} & \text{L} & \frac{\partial P_n}{\partial |V_n|} \\ \frac{\partial Q_2}{\partial \delta_2} & \frac{\partial Q_2}{\partial \delta_3} & \text{L} & \frac{\partial Q_2}{\partial \delta_n} & \frac{\partial Q_2}{\partial |V_2|} & \frac{\partial Q_2}{\partial |V_3|} & \text{L} & \frac{\partial Q_2}{\partial |V_n|} \\ \frac{\partial Q_3}{\partial \delta_2} & \frac{\partial Q_3}{\partial \delta_3} & \text{L} & \frac{\partial Q_3}{\partial \delta_n} & \frac{\partial Q_3}{\partial |V_2|} & \frac{\partial Q_3}{\partial |V_3|} & \text{L} & \frac{\partial Q_3}{\partial |V_n|} \\ \text{M} & \text{M} & \text{M} & \text{M} & \text{M} & \text{M} & \text{M} & \text{M} \\ \frac{\partial Q_n}{\partial \delta_2} & \frac{\partial Q_n}{\partial \delta_3} & \text{L} & \frac{\partial Q_n}{\partial \delta_n} & \frac{\partial Q_n}{\partial |V_2|} & \frac{\partial Q_n}{\partial |V_3|} & \text{L} & \frac{\partial Q_n}{\partial |V_n|} \end{bmatrix} \begin{bmatrix} \Delta \delta_2 \\ \Delta \delta_3 \\ \text{M} \\ \text{M} \\ \Delta \delta_n \\ \Delta |V_2| \\ \Delta |V_3| \\ \text{M} \\ \text{M} \\ \Delta |V_n| \end{bmatrix} \tag{2.1}$$

$$\begin{bmatrix} \frac{\partial P_2}{\partial \delta_2} & \frac{\partial P_2}{\partial \delta_3} & \text{L} & \frac{\partial P_2}{\partial \delta_n} & \frac{\partial P_2}{\partial |V_2|} & \frac{\partial P_2}{\partial |V_3|} & \text{L} & \frac{\partial P_2}{\partial |V_n|} \\ \frac{\partial P_3}{\partial \delta_2} & \frac{\partial P_3}{\partial \delta_3} & \text{L} & \frac{\partial P_3}{\partial \delta_n} & \frac{\partial P_3}{\partial |V_2|} & \frac{\partial P_3}{\partial |V_3|} & \text{L} & \frac{\partial P_3}{\partial |V_n|} \\ \text{M} & \text{M} & \text{M} & \text{M} & \text{M} & \text{M} & \text{M} & \text{M} \\ \frac{\partial P_n}{\partial \delta_2} & \frac{\partial P_n}{\partial \delta_3} & \text{L} & \frac{\partial P_n}{\partial \delta_n} & \frac{\partial P_n}{\partial |V_2|} & \frac{\partial P_n}{\partial |V_3|} & \text{L} & \frac{\partial P_n}{\partial |V_n|} \\ \frac{\partial Q_2}{\partial \delta_2} & \frac{\partial Q_2}{\partial \delta_3} & \text{L} & \frac{\partial Q_2}{\partial \delta_n} & \frac{\partial Q_2}{\partial |V_2|} & \frac{\partial Q_2}{\partial |V_3|} & \text{L} & \frac{\partial Q_2}{\partial |V_n|} \\ \frac{\partial Q_3}{\partial \delta_2} & \frac{\partial Q_3}{\partial \delta_3} & \text{L} & \frac{\partial Q_3}{\partial \delta_n} & \frac{\partial Q_3}{\partial |V_2|} & \frac{\partial Q_3}{\partial |V_3|} & \text{L} & \frac{\partial Q_3}{\partial |V_n|} \\ \text{M} & \text{M} & \text{M} & \text{M} & \text{M} & \text{M} & \text{M} & \text{M} \\ \frac{\partial Q_n}{\partial \delta_2} & \frac{\partial Q_n}{\partial \delta_3} & \text{L} & \frac{\partial Q_n}{\partial \delta_n} & \frac{\partial Q_n}{\partial |V_2|} & \frac{\partial Q_n}{\partial |V_3|} & \text{L} & \frac{\partial Q_n}{\partial |V_n|} \end{bmatrix} \tag{2.2}$$

Jacobean Matrix (2.2) can be divided into four parts J_{11}, J_{12}, J_{21}, J_{22}, which have different physical meanings.

$$J_{11} = \frac{\partial P}{\partial \delta} = \begin{bmatrix} \frac{\partial P_2}{\partial \delta_2} & \frac{\partial P_2}{\partial \delta_3} & \text{L} & \frac{\partial P_2}{\partial \delta_n} \\ \frac{\partial P_3}{\partial \delta_2} & \frac{\partial P_3}{\partial \delta_3} & \text{L} & \frac{\partial P_3}{\partial \delta_n} \\ \text{M} & \text{M} & \text{M} & \text{M} \\ \frac{\partial P_n}{\partial \delta_2} & \frac{\partial P_n}{\partial \delta_3} & \text{L} & \frac{\partial P_n}{\partial \delta_n} \end{bmatrix} \tag{2.3}$$

$$J_{12} = \frac{\partial P}{\partial |V|} = \begin{bmatrix} \frac{\partial P_2}{\partial |V_2|} & \frac{\partial P_2}{\partial |V_3|} & \text{L} & \frac{\partial P_2}{\partial |V_n|} \\ \frac{\partial P_3}{\partial |V_2|} & \frac{\partial P_3}{\partial |V_3|} & \text{L} & \frac{\partial P_3}{\partial |V_n|} \\ \text{M} & \text{M} & \text{M} & \text{M} \\ \frac{\partial P_n}{\partial |V_2|} & \frac{\partial P_n}{\partial |V_3|} & \text{L} & \frac{\partial P_n}{\partial |V_n|} \end{bmatrix} \tag{2.4}$$

$$J_{21} = \frac{\partial Q}{\partial \delta} = \begin{bmatrix} \frac{\partial Q_2}{\partial \delta_2} & \frac{\partial Q_2}{\partial \delta_3} & \text{L} & \frac{\partial Q_2}{\partial \delta_n} \\ \frac{\partial Q_3}{\partial \delta_2} & \frac{\partial Q_3}{\partial \delta_3} & \text{L} & \frac{\partial Q_3}{\partial \delta_n} \\ \text{M} & \text{M} & \text{M} & \text{M} \\ \frac{\partial Q_n}{\partial \delta_2} & \frac{\partial Q_n}{\partial \delta_3} & \text{L} & \frac{\partial Q_n}{\partial \delta_n} \end{bmatrix} \tag{2.5}$$

$$J_{22} = \frac{\partial Q}{\partial |V|} = \begin{bmatrix} \frac{\partial Q_2}{\partial |V_2|} & \frac{\partial Q_2}{\partial |V_3|} & \text{L} & \frac{\partial Q_2}{\partial |V_n|} \\ \frac{\partial Q_3}{\partial |V_2|} & \frac{\partial Q_3}{\partial |V_3|} & \text{L} & \frac{\partial Q_3}{\partial |V_n|} \\ \text{M} & \text{M} & \text{M} & \text{M} \\ \frac{\partial Q_n}{\partial |V_2|} & \frac{\partial Q_n}{\partial |V_3|} & \text{L} & \frac{\partial Q_n}{\partial |V_n|} \end{bmatrix} \tag{2.6}$$

Based on equation (2.3) - (2.6), (2.1) can be rewritten as

$$\begin{bmatrix} \Delta P \\ \Delta Q \end{bmatrix} = \begin{bmatrix} \frac{\partial P}{\partial \delta} & \frac{\partial P}{\partial |V|} \\ \frac{\partial Q}{\partial \delta} & \frac{\partial Q}{\partial |V|} \end{bmatrix} \begin{bmatrix} \Delta \delta \\ \Delta |V| \end{bmatrix} \tag{2.7}$$

Once the power system steady state has been calculated by solving power non-linear equations, the inverse of the Jacobean Matrix can also be obtained whose structure as follows.

$$\begin{bmatrix} \frac{\partial \delta_2}{\partial P_2} & \frac{\partial \delta_2}{\partial P_3} & \text{L} & \frac{\partial \delta_2}{\partial P_n} & \frac{\partial \delta_2}{\partial Q_2} & \frac{\partial \delta_2}{\partial Q_3} & \text{L} & \frac{\partial \delta_2}{\partial Q_n} \\ \frac{\partial \delta_3}{\partial P_2} & \frac{\partial \delta_3}{\partial P_3} & \text{L} & \frac{\partial \delta_3}{\partial P_n} & \frac{\partial \delta_3}{\partial Q_2} & \frac{\partial \delta_3}{\partial Q_3} & \text{L} & \frac{\partial \delta_3}{\partial Q_n} \\ \text{M} & \text{M} & \text{M} & \text{M} & \text{M} & \text{M} & \text{M} & \text{M} \\ \frac{\partial \delta_n}{\partial P_2} & \frac{\partial \delta_n}{\partial P_3} & \text{L} & \frac{\partial \delta_n}{\partial P_n} & \frac{\partial \delta_n}{\partial Q_2} & \frac{\partial \delta_n}{\partial Q_3} & \text{L} & \frac{\partial \delta_n}{\partial Q_n} \\ \frac{\partial |V_2|}{\partial P_2} & \frac{\partial |V_2|}{\partial P_3} & \text{L} & \frac{\partial |V_2|}{\partial P_n} & \frac{\partial |V_2|}{\partial Q_2} & \frac{\partial |V_2|}{\partial Q_3} & \text{L} & \frac{\partial |V_2|}{\partial Q_n} \\ \frac{\partial |V_3|}{\partial P_2} & \frac{\partial |V_3|}{\partial P_3} & \text{L} & \frac{\partial |V_3|}{\partial P_n} & \frac{\partial |V_3|}{\partial Q_2} & \frac{\partial |V_3|}{\partial Q_3} & \text{L} & \frac{\partial |V_3|}{\partial Q_n} \\ \text{M} & \text{M} & \text{M} & \text{M} & \text{M} & \text{M} & \text{M} & \text{M} \\ \frac{\partial |V_n|}{\partial P_2} & \frac{\partial |V_n|}{\partial P_3} & \text{L} & \frac{\partial |V_n|}{\partial P_n} & \frac{\partial |V_n|}{\partial Q_2} & \frac{\partial |V_n|}{\partial Q_3} & \text{L} & \frac{\partial |V_n|}{\partial Q_n} \end{bmatrix} \begin{bmatrix} \Delta P_2 \\ \Delta P_3 \\ \text{M} \\ \text{M} \\ \Delta P_n \\ \Delta Q_2 \\ \Delta Q_3 \\ \text{M} \\ \text{M} \\ \Delta Q_n \end{bmatrix} = \begin{bmatrix} \Delta \delta_2 \\ \Delta \delta_3 \\ \text{M} \\ \text{M} \\ \Delta \delta_n \\ \Delta |V_2| \\ \Delta |V_3| \\ \text{M} \\ \text{M} \\ \Delta |V_n| \end{bmatrix} \quad (2.8)$$

Inverse of Jacobean Matrix can be written as $[J]^{-1}$, which is called Sensitivity Matrix.[12]

This matrix basically describes the impact on the voltage magnitude and angle of each bus, due to a change in active/reactive power at some location, like a bus. And the phase angle is directly related with frequency. If the frequency at two buses are same the phase angle difference between them will stay same otherwise it will change. So once a real power change, Δ P, happens, we can measure its affect to entire system by observing the voltage magnitude and frequency of each bus.

As mentioned above, the influences caused by Δ P to bus voltage magnitude and frequency are non-linear. So the size of PL need to have different ranges, and the most effective bus maybe variable according to different ranges of PL.

3.1 Voltage Sensitivity Analysis

The most voltage effective bus is one whose real power change significantly influences the voltage of every node in the system. In order to find the most effective bus, this research added the real power load, P_L, to every node of the 34-bus system respectively, except the swing bus 800. For each simulation, the real power load can be added at only one bus by changing the size of the P_L to simulate the charge and discharge processes of the battery. Increasing the real power load can be regarded as the charging process of the ESS, while the discharging process represents decreasing the load size.

This study hypothesized that adding the active power load to a certain node has the same effect on change in real power as adding the real power source at the bus. In the simulation, the stable voltage of each bus was recorded after each 40 Kw size change of the P_L from 0 kW to the peak value 160 Kw. Afterwards, the voltage was measured in reverse order from 160 kw to 0 Kw in 40 kw increments. 160 kW was set as the peak value as it is close to the critical value which cause the voltage of the entire system to collapse. For example, adding the real power load P_L to bus 852. Recording the stable voltage of each bus after every size change of the P_L. See the figure 3.1-3.6 for details, and in each figures the abscissa means the size of P_L, the unit is kW, while the ordinate represents the corresponding bus stable voltage in per unit.

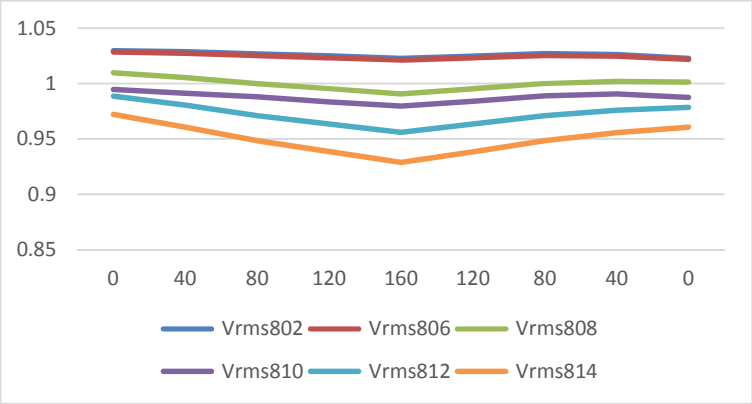

Fig. 3-1

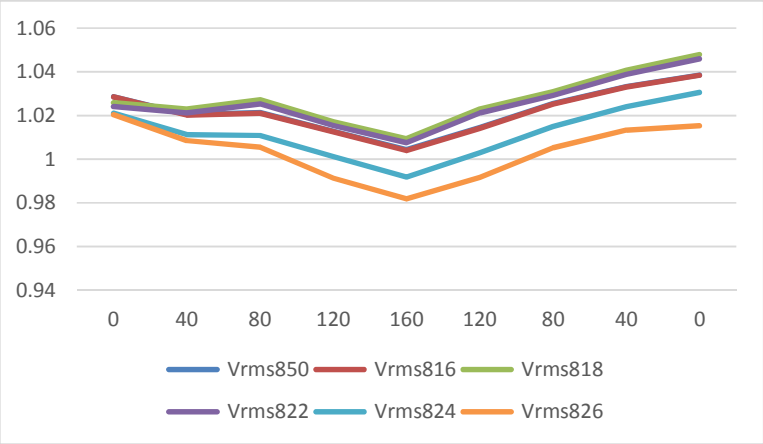

Fig. 3-2

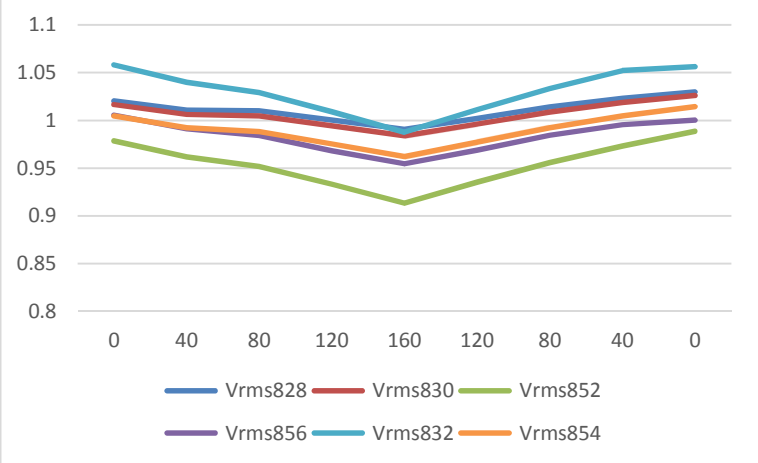

Fig. 3-3

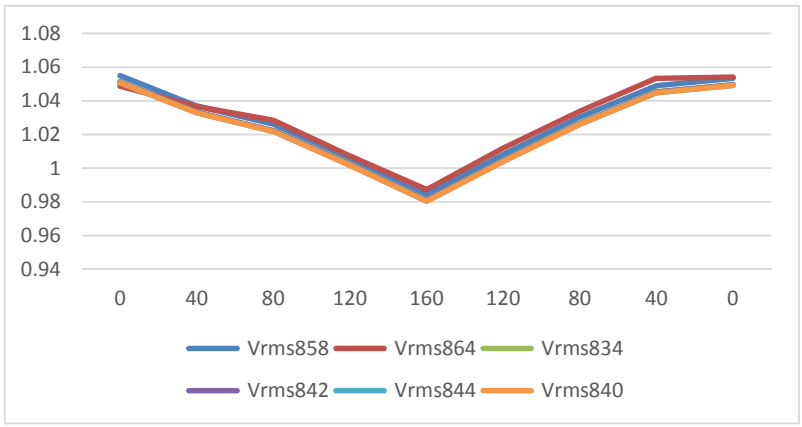

Fig. 3-4

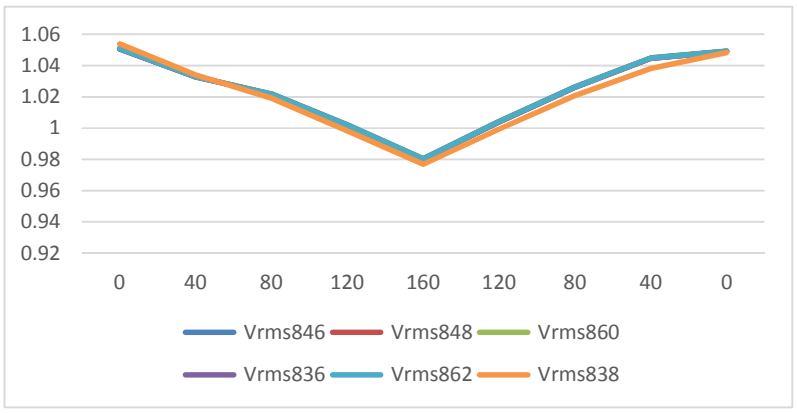

Fig. 3-5

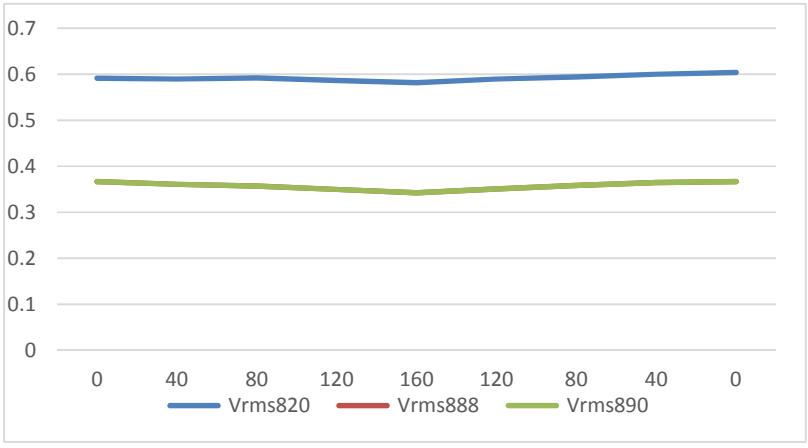

Fig. 3-6

These figures show the voltage change of 33 buses, except the swing bus 800, when the size of P_L at bus 852 changed directly.

There are some points need to be cleared:

1) In order to find the most effective bus more directly, the two wind turbines are not connected to the system in these simulations, so we can avoid the fluctuations wind turbines bring.

2) In the above figures, the horizontal coordinate means the size of the real power load, some numbers have the same value, but their meanings are different. For example, from left to right, the second and penultimate numbers are both '40', but they have different bases. The first '40' kW is based on 0 kW, while the second '40' kW is based on 80 kW.

3) Some Simulation results show that when the size of P_L added at the single-phase bus becomes larger, some voltage magnitude of other single-phase buses will increase, but not decrease. Take the single-phase node 810 as an example, and it is on phase B. When the P_L added at 810 becomes larger, the voltage magnitudes of the bus 822 and bus 820 which are on phase A increased. It probably because these buses are on different phases. When P_L increased at bus 810, the need for real power of phase B became larger. Generators output more real power to make up for this power deficiency. But this compensatory real power generated by the diesel was three-phase, so the real power in phases A and C became relative "surplus", leading voltage of phase A and C slightly increase.

Except the swing node, adding the variable-size P_L at some bus, the voltage change, ΔV, of every bus in different P_L ranges can be obtained. The parameter V need to be

introduced here to measure the sensitivity of the bus voltage. V is equal to the root mean square of the voltage magnitude changes for 33 nodes. And for each ΔV, its initial voltage magnitude is regarded as the reference. It is cleared that the larger V is, the bigger influence one node has in certain PL range. Then choose another bus to add the size-changing PL, again measuring all the stable bus voltage magnitudes until all buses had been added with PL. In this way, the most influent bus in every different PL ranges can be found respectively.

$$\Delta V_{bus\ A} = V_{bus\ A} - V_{initial\ value\ of\ bus\ A} \quad (3\text{-}1)$$

$$\mathrm{V} = \sqrt[2]{(\Delta V_{802})^2 + (\Delta V_{806})^2 + \ldots (\Delta V_{814})^2 + \cdots + (\Delta V_{890})^2} \quad (3\text{-}2)$$

For example, adding the real power load at bus 852, and changing the size of PL from 0 kW to 40 kW, the voltage changes of 33 nodes are as follow:

Table 3.1 the voltage change of every node when the PL changes from 0 kW to 40 kW at node 852

node	802	806	808	810	812
ΔV	0.0733	0.0905	0.4182	0.3308	0.8179
node	814	850	816	818	822
ΔV	1.1492	0.8121	0.8168	0.2925	0.2864
node	824	826	828	830	852
ΔV	0.9697	1.1818	0.9824	1.0395	1.665
node	856	832	854	858	864
ΔV	1.4235	1.8008	1.2202	1.7934	1.2112
node	834	842	844	840	846
ΔV	1.7853	1.78	1.7832	1.7856	1.7822
node	848	860	836	862	838
ΔV	1.782	1.7854	1.7856	1.7856	1.7856
node	820	888	890		
ΔV	0.1655	0.6242	0.6242		

Notes：each value of ΔV has been multiplied by 100.

So, the corresponding V for range 0-40 kW is obtained,

$$V = \sqrt[2]{(\Delta V_{802})^2 + (\Delta V_{806})^2 + \ldots (\Delta V_{814})^2 + \cdots + (\Delta V_{890})^2} = 0.013003$$

when the PL added at all different buses respectively and the size of PL changed from 0 kW to 40 Kw, comparing the different values of V, then the relative infective buses can be found in this range.

Table 3-2 the most five voltage effective buses in the PL range from 0 kW to 40 kW

node	840	862	836	860	844
V	1.3707	1.3703	1.3698	1.3621	1.3588

Notes：each value of ΔV has been multiplied by 100.

Similarly, when PL changes from 0 kW to 80 kW, the relative influent buses can be found in this range.

There are some points need to be cleared:

1) Through the simulation, it is found that the PL change at single-phase bus causes relative small voltage magnitude changes compared with the three-phase nodes. So the single-phase buses are not regarded as candidate bus where the ESS plans to be in-stored.

2) As can be seen from Fig. 3.1-3.6, the influence of PL to the bus voltage magnitude is symmetrical to each bus, so this research only considered the increasing part of PL when deciding the size of ESS.

The most five voltage effective candidate buses can be found in different PL ranges

respectively. As shown in table 3.3.

Table 3.3

The change of PL	The five most voltage effective nodes in different ranges of PL				
0 kW-40 kW	V_{840}=1.3707	V_{862}=1.3703	V_{836}=1.3698	V_{860}=1.3621	V_{844}=1.3588
0 kW-80 kW	V_{840}=2.5502	V_{862}=2.4175	V_{836}=2.4172	V_{860}=2.4009	V_{842}=2.3853
0 kW-120 kW	V_{848}=3.8255	V_{846}=3.8225	V_{844}=3.7901	V_{840}=3.6783	V_{862}=3.6783
0 kW-160 kW	V_{860}=5.5407	V_{844}=5.5009	V_{862}=5.4961	V_{836}=5.493	V_{840}=5.4928

Notes：each value of ΔV has been multiplied by 100.

3.2 Frequency Sensitivity Analysis

Similarly, the most frequency effective bus is one whose real power change significantly influences the frequency of every node in the system. In order to find the most effective bus, this research added the real power load, P_L, to every node of the 34-bus system respectively, except the swing bus 800. The PL was added at only one bus for each simulation.

In the simulation, the size of the P_L was changed similarly as the voltage analysis above, the upper bound 160 kW was set for the similar reason. The stable frequency was recorded after every size change of the P_L. For example, adding the P_L at bus 802. Recording the stable frequency after every size change of the P_L. See the figure 3.7 for details, and for each figure the abscissa represents the size of P_L while the ordinate means the corresponding actual value of system frequency.

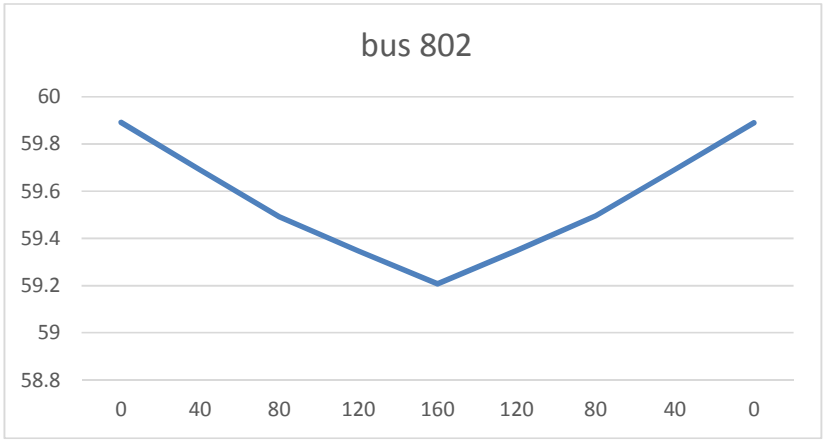

Fig. 3.7

But here are some differences with the voltage sensitivity analysis.

1) Since it was a microgrid, the frequency differences among all the nodes were very small, so the frequency at node 802 was chosen as the system frequency.
2) The voltage magnitude were in per-unit without any unit, while unit of system frequency is hertz.

Then adding the size-changing PL at other buses respectively, recording the corresponding system frequency. See Figure 3.8-3.11 for details.

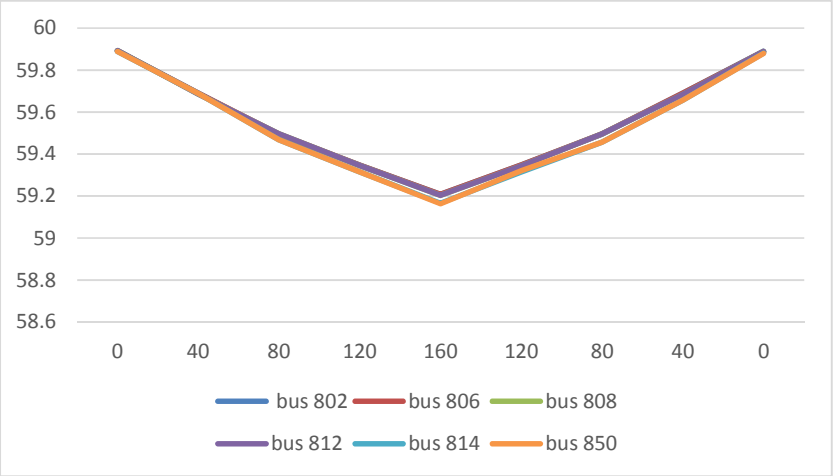

Fig. 3.8

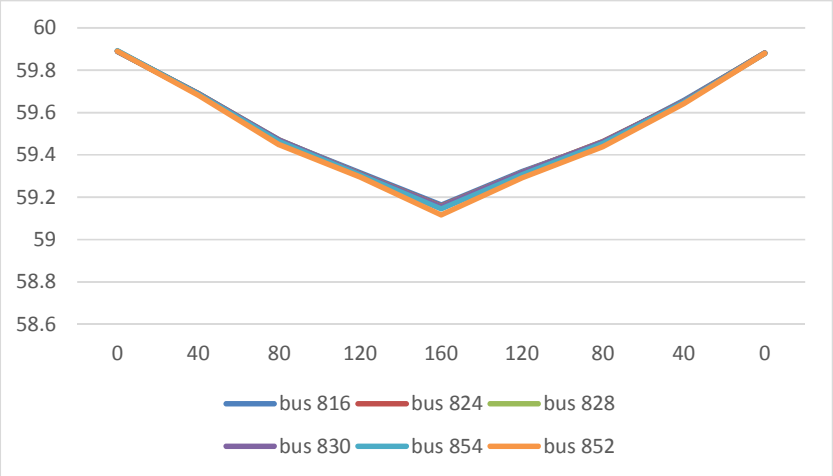

Fig. 3.9

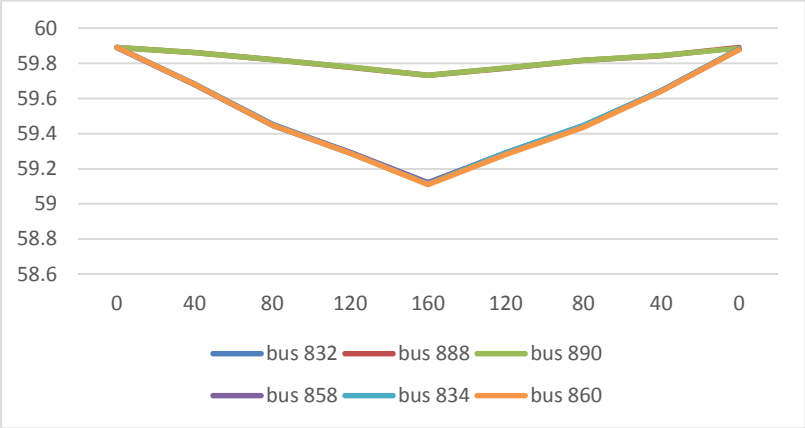

Fig. 3.10

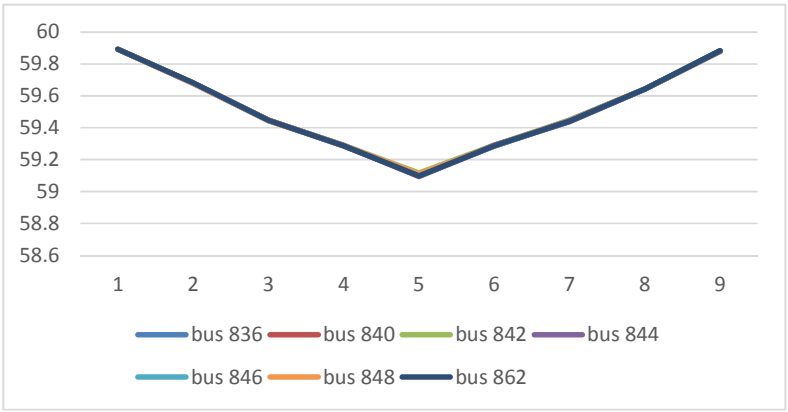

Fig. 3.11

Except the swing node, adding the varying-size PL at some three-phase bus, the system frequency change, ΔF, can be obtained in different real power load ranges. And for every size change of PL at a certain bus, there is only one ΔF will be obtained, so it was directly used to measure the frequency effectivity. The larger ΔF means the larger frequency influence one node has in a certain real power range. Then choose another bus to add the size-changing PL, again measuring the system voltage until all candidate

buses had been added with PL. In this way, the most frequency influent bus in different PL ranges can be found respectively.

Table 3.4

The range of PL	The most five frequency effective nodes in different PL ranges				
0Kw-40kW	ΔF_{848}=2.1362	ΔF_{846}=2.1350	ΔF_{862}=2.1080	ΔF_{836}=2.1080	ΔF_{840}=2.1063
0Kw-80kW	ΔF_{846}=4.4683	ΔF_{848}=4.4610	ΔF_{844}=4.4608	ΔF_{836}=4.4483	ΔF_{862}=4.4474
0Kw-120kW	ΔF_{840}=6.0549	ΔF_{836}=6.0415	ΔF_{862}=6.0408	ΔF_{860}=6.0394	ΔF_{834}=6.0343
0Kw-160kW	ΔF_{844}=7.9619	ΔF_{846}=7.9393	ΔF_{860}=7.9202	ΔF_{840}=7.8995	ΔF_{860}=7.8765

Notes：each value of ΔF has been multiplied by 10.

In order to observe the real power's combined effect to both voltage and frequency at a certain node, the ΔF above is converted in per-unit and listed in table 3.5.

Table 3.5

The change of PL	The most five frequency effective nodes in different ranges of PL				
0Kw-40kW	ΔF_{846}=0.356029	ΔF_{848}=0.355835	ΔF_{862}=0.351338	ΔF_{836}=0.351326	ΔF_{840}=0.351048
0Kw-80kW	ΔF_{846}=0.744715	ΔF_{848}=0.743494	ΔF_{844}=0.743461	ΔF_{836}=0.741389	ΔF_{862}0.741233
0Kw-120kW	ΔF_{840}=1.009144	ΔF_{836}=1.006911	ΔF_{862}=1.006805	ΔF_{860}=1.006562	ΔF_{834}=1.005712
0Kw-160kW	ΔF_{844}=1.326986	ΔF_{846}=1.323212	ΔF_{860}=1.320026	ΔF_{840}=1.316586	ΔF_{860}=1.3212744

Notes：each value of ΔF has been multiplied by 100.

4 reliability analysis

4.1 Reliability Indexes Introduction

SAIFI, the system average interruption frequency index, is commonly used as a reliability indicator by electric power utilities. Generally, it is measured in units of interruptions per customer over the course of a year. Here, it means the number of interruptions per bus over the course of the simulation.

$$\text{SAIFI} = \frac{\textbf{\textit{Total number of customer interruptions}}}{\textbf{\textit{Total number of customers served}}}$$

SAIFI is improved by reducing the frequency of outages (for example, by tree trimming). SAIFI is also improved by reducing the number of customers interrupted when outages do occur (for example, by adding reclosers, sectionalizing overcurrent protective devices, and fuses).

SAIDI, the system average interruption duration index, also is commonly used as a reliability indicator by electric power utilities. It is the average outage duration for each customer served and is measured in units of time, often minutes or hours, over the course of a year. Here it is measured over the course of each simulation.

$$\text{SAIDI} = \frac{\textbf{\textit{Sum of all customer interruption durations}}}{\textbf{\textit{Total number of customers served}}}$$

Strategies that reduce SAIFI improve SAIDI because if an outage does not happen, it doesn't add to duration. Both SAIFI and SAIDI can be reduced by preventing sustained outages. Approximately 75 percent of overhead faults have a temporary cause such as lightning, animals, trees or debris in the line, or vehicles hitting poles causing conductors to slap together. SAIDI is also improved through faster customer restoration,

but not SAIFI.

Customer Average Interruption Duration Index, CAIDI, is related to SAIDI and SAIFI. It gives the average outage duration that any involved customer would experience per sustained interruption, and it can also be viewed as the average restoration time. CAIDI is measured in units of time, often minutes or hours over the course of a year. Improving SAIFI and SAIDI can sometimes adversely affect CAIDI.

$$\text{CAIDI} = \frac{Sum\ of\ all\ customer\ interruption\ durations}{Total\ number\ of\ customer\ interruptions}$$

$$= \frac{Sum\ of\ all\ customer\ interruption\ durations}{Total\ number\ of\ customers\ served} * \frac{Total\ number\ of\ customers\ served}{Total\ number\ of\ customer\ interruptions}$$

$$= \frac{SAIDI}{SAIFI}$$

Customer Total Average Interruption Duration Index, CTAIDI, the average total duration of interruption for customers who had at least one interruption during the period of analysis, and customers with multiple interruptions are counted only once.

$$\text{CTAIDI} = \frac{Sum\ of\ all\ customer\ interruption\ durations}{Number\ of\ distinct\ customers\ interrupted}$$

CTAIDI is measured in units of time, such as minutes or hours. It is similar to CAIDI, but CAIDI divides the total duration of interruptions by the number of interruptions whereas CTAIDI divides by the number of interrupted customers. When CTAIDI is much greater than CAIDI, the service outages are more concentrated among certain customers.

$$\frac{SAIDI}{CTAIDI} = \frac{SAIFI}{CAIFI}$$

This research also introduced another indicator, the integration the exceeding part of voltage over the time. The voltage magnitude's normal range is from 0.95 to 1.05 in per unit. When the voltage exceeds this range, the exceeding part will be integrated over the time, as shown in the fig. 4.1, the red shaded part. And according to fig. 4.1, the interruption happens twice, and the interruption duration equals to $t1+t2$.

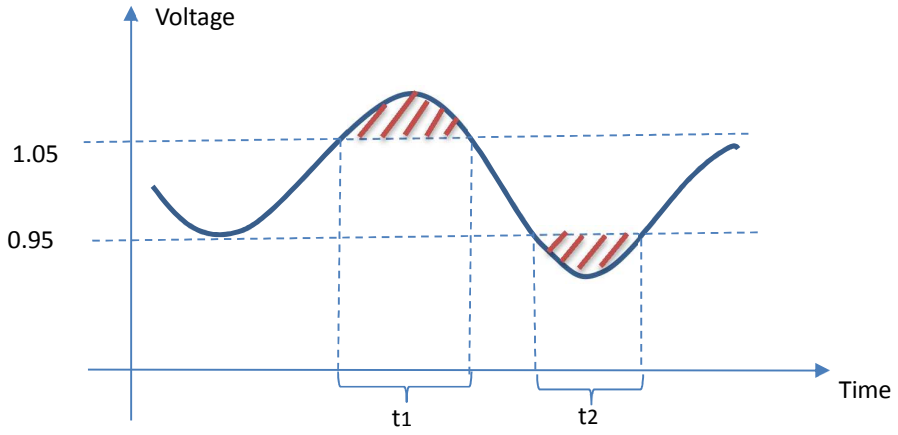

4.2 Case Study

The sampling frequency both of voltage and frequency were 100 times per second in simulation. Once the voltage in per unit was over 1.05 or less than 0.95, or system frequency was over 60.5 hertz or less than 59.5 hertz was regarded as an interruption, regardless of the duration. For each simulation, the course were 30 seconds, but the first six seconds were omitted due to the shock caused by the generator starting, so the actual recording time were 24 seconds.

4.21 Battery at Bus 846

Five indexes mentioned above are used to measure the change of bus voltage in the research. Considering the results of the voltage and frequency sensitivity analysis in the previous chapter, when the real power load range was from 0 kW to 120 kW, the most effective bus was 846. And it was chosen to add one energy storage battery with 120 kW maximum real power output. By the way, bus 840 and 848 were connected to two wind turbines respectively. Then the simulation data were gotten, as shown in table 4.1.

Table 4.1

Bus	806	808	810	802	812	814	824	822
interruptions	6	6	117	6	4	3	23	161
duration	1.69	1.93	1.49	1.68	2.13	2.23	1.11	2.18
integration	1.79166	2.33442	3.52020	1.77229	3.31659	4.43830	0.47126	2.79324
Bus	820	818	850	816	856	854	830	828
interruption	161	182	18	19	141	11	11	28
duration	2.18	2.56	0.63	0.64	2.33	2.12	2.11	1.19
integration	2.79763	3.20998	0.28127	0.28264	6.29374	1.95237	1.89994	0.50337
Bus	832	848	846	844	834	864	842	826
interruption	20	11	11	10	11	245	11	149
duration	4.36	4.02	4.00	3.97	4.02	7.00	4.00	2.2
integration	12.26591	11.44179	11.37614	11.21308	11.419	18.31927	11.38307	5.050247
Bus	858	840	838	836	862	860	852	
interruption	14	21	204	19	19	14	11	
duration	4.13	4.19	7.42	4.16	4.16	4.07	2.12	
integration	11.8310	12.1526	20.4047	12.0011	11.9984	11.6017	1.952367	

Note: all values of integration were multiplied by 100.

The total number of all buses' interruptions was 1667,

$$\text{SAIFI} = \frac{\textbf{Total number of customer interruptions}}{\textbf{Total number of customers served}} = \frac{\mathbf{1667}}{\mathbf{31}} = 53.7742$$

The sum of all buses' interruptions duration time were 92.02 seconds.

$$\text{SAIDI} = \frac{\textbf{Sum of all customer interruption durations}}{\textbf{Total number of customers served}} = \frac{\mathbf{92.02}}{\mathbf{31}} = 2.96839 \text{ seconds}$$

$$\text{CAIDI} = \frac{Sum\ of\ all\ customer\ interruption\ durations}{Total\ number\ of\ customer\ interruptions} = \frac{SAIDI}{SAIFI} = 0.0552 \text{ seconds}$$

$$\text{CTAIDI} = \frac{Sum\ of\ all\ customer\ interruption\ durations}{Number\ of\ distinct\ customers\ interrupted} = \frac{\mathbf{92.02}}{\mathbf{31}} = 2.96839 \text{ seconds}$$

CTAIDI is much greater than CAIDI means the service outages are more concentrated among certain buses. And the total integration of all exceeding part of voltage over time were 2.120693. As for the system frequency, after the battery was added, the system frequency basically stayed constant at 60 hertz.

4.22 Battery at Bus 860

Based on the sensitivity analysis in the previous chapter, the most effective bus was 860 when the PL was 160 kW. And it was chosen to add one energy storage battery with 160 kW maximum real power output. For the same reason the bus voltage and system frequency were recorded since the 7th second. The same three parameters were used to measure the change of voltage. The data we got were as shown in table 4.2.

Table 4.2

Bus	806	808	810	802	812	814	824	822
interruptions	0	0	54	0	1	17	2	103
duration	0	0	0.54	0	0	0.37	0.79	1.58
integration	0	0	0.424665	0	0	0.062139	0.373694	2.049262

Bus	820	818	850	816	856	854	830	828
interruption	103	121	18	18	116	7	6	2
duration	1.58	1.94	0.52	0.52	1.94	1.01	1.00	0.79
integration	2.057306	2.570809	0.270028	0.270914	3.169473	0.886423	0.867379	0.387277
Bus	832	848	846	844	834	864	842	826
interruption	17	22	24	26	29	126	28	121
duration	4.26	4.59	4.49	4.15	4.19	5.50	4.18	1.84
integration	10.9382	10.44365	10.35776	9.84729	9.941122	15.52411	9.924527	2.382101
Bus	858	840	838	836	862	860	852	
interruption	22	145	145	23	23	30	7	
duration	4.20	6.98	6.98	4.64	4.64	4.31	1.01	
integration	10.42035	10.77421	17.2215	10.55467	10.55154	9.994088	0.886423	

Note: the bus 888 and 890 are not listed and all values the integration were multiplied by 100.

The total number of all buses' interruptions was 1236,

$$\text{SAIFI} = \frac{\textbf{\textit{Total number of customer interruptions}}}{\textbf{\textit{Total number of customers served}}} = \frac{\mathbf{1236}}{\mathbf{31}} = 39.87$$

The sum of all buses' interruptions duration time were 76.33 seconds.

$$\text{SAIDI} = \frac{\textbf{\textit{Sum of all customer interruption durations}}}{\textbf{\textit{Total number of customers served}}} = \frac{\mathbf{76.33}}{\mathbf{31}} = 2.4623 \text{ seconds}$$

$$\text{CAIDI} = \frac{\textit{Sum of all customer interruption durations}}{\textit{Total number of customer interruptions}} = \frac{\textit{SAIDI}}{\textit{SAIFI}} = 0.06176 \text{ seconds}$$

$$\text{CTAIDI} = \frac{\textit{Sum of all customer interruption durations}}{\textit{Number of distinct customers interrupted}} = \frac{\mathbf{76.33}}{\mathbf{31-4}} = 2.827 \text{ seconds}$$

CTAIDI is much greater than CAIDI, the service outages are more concentrated among certain buses. And the total integration of all exceeding part of voltage over time was

1.63151. As for the system frequency, after the battery was added, the system frequency basically stayed constant at 60 hertz.

5 Verifications

5.1 Same Battery Added at Different Buses

For each size of the real power load, buses had been ranked by its influence to voltage and frequency in a descending manner through sensitivity analysis. To verify the rank when the range of real power load is 0 kW to 120 kW, this research chose three typical buses, bus 846 with the most effective influence, bus 832 with general influence and bus 850 with relative poor influence to add one battery. The battery with 120 kW maximum real power output was add at these three buses respectively. Five indexes, mentioned before were used to measure voltage change. And simulation without any battery added in microgrid was also run, which has an effect of contrast. See table 5.1 for detail.

Table 5.1

Bus	846	832	850	Without battery
SAIFI	53.77419	64.22581	70.87097	78.54839
SAIDI	2.968387	3.291613	4.295161	7.266452
CAIDI	0.0552	0.05125	0.0606	0.09251
CTAIDI	2.96839	3.291613	4.295161	7.266452
the value of integration	2.120693	2.182009	2.322626	4.305464

We can see that the more influent the bus is, the smaller SAIFI，SAIDI, CAIDI, CTAIDI and integral values are. In other words, for the same battery, it can suppress the voltage fluctuation caused by the wind turbines better if it is added at the relative more influent bus.

Similarly, according to the rank sorted when the real power load is 160 kW, this research also chose such three representative buses, the most effective influence bus 860, the general influence bus 858 and the relative poor influence bus 808 to add one battery. The battery with 160 kW maximum real power output was add at these three buses respectively. See table 5.2 for detail.

Table 5.2

Bus	860	858	808	Without battery
SAIFI	39.87097	45.64516	51.6129	78.54839
SAIDI	2.462258	3.791935	3.32871	7.266452
CAIDI	0.061756	0.083074	0.064494	0.092509
CTAIDI	2.726071	3.791935	3.685357	7.266452
the value of integration	1.63151	2.266201	2.144582	430.5464

When the maximum real power output of the battery was 160 kW, similar conclusions can be drawn. The bus ranking resulted from the sensitivity analysis corresponded with the results of the verification experiment.

5.2 adding different batteries at the same bus

As mentioned before the battery with 120 kW maximum real power output was added at the most effect bus 846 in this range, and all reliability indexes were obtained. Then changing the maximum real power output of the battery to 160 kW at the same bus, bus 846. By comparing these two sets of indexes, we can know the influence of battery size. See table 5.3 for detail.

Table 5.3

Battery size (Kw)	120	160	Without battery
SAIFI	53.77419	44.83871	78.54839
SAIDI	2.968387	2.917097	7.266452
CAIDI	0.0552	0.065058	0.092509
CTAIDI	2.96839	2.917097	7.266452
the value of integration	2.120693	1.988141	430.5464

Keep the location same to add the battery same, and only change the real power output of the battery. It is obvious that the battery with larger maximum real power impresses the fluctuations of voltage better.

6 conclusions

This research proposes a novel method of how to integrate controlling parameters, voltage and frequency, into to the ESS allocation in a microgrid with renewable sources. First, sensitivity analysis is used to rank all the buses according to their influences. Accessing the battery at more influent bus can minimize the fluctuations caused by the uncertainty of wind speed better. Reliability analysis based on controlling parameters can further help to decide the optimum allocation of the ESS. Indicators, such as SAIDI and SAIFI, are used to measure the system reliability after the size and location of ESS are determined.

The results obtained by above two analysis methods correspond with each other. Considering controlling parameter in planning is an effective way in the allocation of ESS.

References

[1] G. W. E. Council. (2014). Global Wind Energy Outlook 2014 [Online]. Available: http://www.gwec.net/wp-content/uploads/2014/10/GWEO2014_WEB.pdf.

[2] A. S. A. Awad, T. H. M. El-Fouly, and M. M. A. Salama, "Optimal ESS Allocation and Load Shedding for Improving Distribution System Reliability," to appear at IEEE Transactions on Smart Grid.

[3] C. Abbey and G. Joos, "A Stochastic Optimization Approach to Rating of Energy Storage Systems in Wind-Diesel Isolated Grids," IEEE Transactions on Power Systems, vol. 24, no. 1, pp. 418-426, Feb. 2009.

[4] S. X. Chen, H. B. Gooi, and M. Q. Wang, "Sizing of Energy Storage for Microgrids," IEEE Transactions on Smart Grid, vol. 3, no. 1, pp. 142151, Mar. 2012.

[5] M. Korpaas, A. T. Holen, and R. Hildrum, "Operation and sizing of energy storage for wind power plants in a market system," International Journal of Electrical Power & Energy Systems, vol. 25, no. 8, pp. 599606, Oct. 2003.

[6] R. C. Dugan and W. H. Kersting, “Induction machine test case for the34-bus test feeder - description,” in Proc. IEEE Power Eng. Soc. Gen. Meet., Montreal, QC, Canada, 2006, pp. 1–4.

[7] N. Samaan, T. McDermott, B. Zavadil, and J. Li, “Induction machine test case for the 34-bus test feeder—Steady state and dynamic solutions,” in Proc. IEEE Power Eng. Soc. Gen. Meet., Montreal, QC, Canada, 2006, pp. 1–5.

[8] Q. Fu, L. F. Montoya, A. Solanki, A. Nasiri, V. Bhavaraju, T. Abdallah, and D. C. Yu, “Microgrid generation capacity design with renewable and energy storage addressing power quality and surety,” IEEE Trans. Smart Grid, vol. 3, pp. 2019–2027, 2012.

[9] Q. Fu, L. F. Montoya, A. Solanki, A. Nasiri, V. Bhavaraju, T. Abdallah, and D. C. Yu, “Generation capacity design for a microgrid for measurable power quality indexes,” in Proc. IEEE ISGT 2012 Conf., Washington, D.C., USA, pp. 1–6.

[10] E. Manla, A. Nasiri, C. Rentel, and M. Hughes, “Modeling of zinc bromide energy storage for vehicular applications,” IEEE Trans. Ind. Electron., vol. 57, no. 2, pp. 624–632, 2010.

[11] A. Solanki, Q. Fu, L. F. Montoya, A. Nasiri, V. Bhavaraju, T. Abdallah, and D. C. Yu, “Managing intermittent renewables in a microgrid,” in Proc. IEEE ISGT 2012 Conf., Washington, D. C., USA, pp.1–6.

[12] Luis Fernando Montoya Sanchez, “Novel methodology to determine the optimal energy storage location in a microgrid to support power stability”, The University of Wisconsin-Milwaukee, December 2012.